Interpreting "Acidity" as a Global Property Controlling Comonomer Reactivity in Olefin Polymerization

Lorella Izzo*

Dipartimento di Chimica e Biologia, Università degli Studi di Salerno, via Giovanni Paolo II, 132, 84084 Fisciano, Italy

Massimo Mella*

Dipartimento di Scienza ed Alta Tecnologia, Università degli Studi dell'Insubria, via Valleggio 11, 22100 Como, Italy

S *Supporting Information*

ABSTRACT: A possible rationale for the different catalytic behaviors of systems based on *rac*-(ethylenebis(1-indenyl)) zirconium dichloride (*rac*-EBIZrCl$_2$), *rac*-(ethylenebis(1-indenyl))hafnium dichloride (*rac*-EBIHfCl$_2$), and *rac*-(isopropylidenebis(1-indenyl))zirconium dichloride (*rac*-iPr-BIZrCl$_2$) toward ethene−styrene copolymerization has been sought by studying related active systems. For this purpose, the metallocene ion pairs (IPs) *rac*-EBIZrMe—MeB(C$_6$F$_5$)$_3$, *rac*-EBIHfMe—MeB(C$_6$F$_5$)$_3$, and *rac*-iPrBIZrMe—MeB(C$_6$F$_5$)$_3$ have been synthesized and their structures in solution explored with ROESY and pulsed gradient NMR spectroscopy. The energetics of dynamical processes relevant for catalysis that can

be used as indicators of the cation acidity have been studied with variable-temperature NMR experiments and density functional theory (DFT). NMR experiments successfully provided IP structural details in solution and also indicated the presence of an intricate dynamic behavior for all the IPs. DFT results, instead, indicated quantitatively how changing the metal and/or the ancillary ligand bridge influences the energetics of the active species and modifies the reaction energy profile. The theoretical results also drew attention to the fact that finding a rationale for the ligand influence on the catalytic behavior of *rac*-EBIZrCl$_2$/ MAO and *rac*-iPrBIZrCl$_2$/MAO in ethene−styrene copolymerization requires not only considering the steric effects but also determining how subtle changes in the ligand sphere affect the capability of the metal center to accept electrons from the counteranion or the olefins.
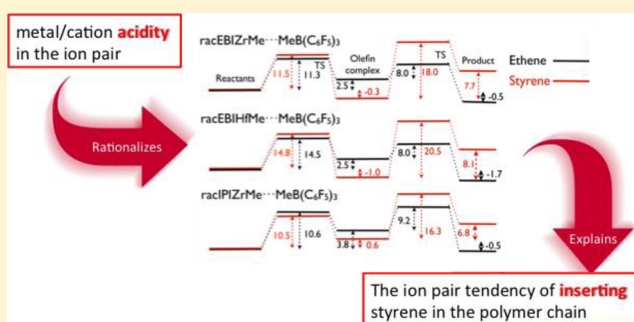
■ INTRODUCTION

It is known from the literature that *rac*-(ethylenebis(1-indenyl))zirconium dichloride (*rac*-EBIZrCl$_2$), *rac*-(ethylenebis(1-indenyl))hafnium dichloride (*rac*-EBIHfCl$_2$), and *rac*-(isopropylidenebis(1-indenyl))zirconium dichloride (*rac*-iPrBIZrCl$_2$) activated by a strong Lewis acid produce anything from random to alternating ethene−styrene copolymers. Under similar experimental conditions (i.e., temperature and feed composition), the three catalysts show an increasing capability to insert styrene into the polymer backbone, following the order *rac*-EBIZrCl$_2$ < *rac*-EBIHfCl$_2$ < *rac*-iPrBIZrCl$_2$. So far, the different behaviors between *rac*-EBIZrR$^+$ and *rac*-iPrBIZrR$^+$ active complexes have been justified as being due to structural differences, the smaller steric encumbrance of the ligands on the metal in the latter cation being held responsible for the increased reactivity toward the bulkier styrene. This interpretation, however, does not explain how the more encumbered metal center in *rac*-EBIZrR$^+$ appears to increase its relative reactivity toward styrene upon lowering the temperature, so much so that it becomes able to produce an almost alternating ethene−styrene copolymer only when

cooled to −25 °C,[1] while the *rac*-iPrBIZrR$^+$-based catalyst inserts substantially more styrene already at a higher temperature.[2] Given the similarities in the structures, simple steric effects seem also unable to justify the difference in ethene−styrene reactivities at 50 °C between *rac*-EBIZrCl$_2$ and *rac*-EBIHfCl$_2$, the latter being capable of inserting much more styrene under such conditions (Table 1).

Clearly, a more complete understanding of the links between the catalyst features (e.g. geometrical structure and acidity of the metal center) and the differences in catalytic behavior toward monomers with different basicities or nucleophilicities would be beneficial when it comes to designing systems with modulated reactivity. As an example, it is mentioned here that a theoretical analysis succeeded in a priori exploring the possible change in reactivity with respect to ethene oligomerization and polymerization catalyzed by [OSSO]-type complexes upon modification of the coordinated metal.[3] It is thus with such purpose in mind that we approached the task of rationalizing

**Table 1. Styrene Content in Ethene−Styrene Copolymers and in the Polymerization Feed at Different Temperatures**

catalyst precursor	T_{polm} (°C)	$[E]/[S]_{feed}$	X_S
rac-EBIZrX$_2$	−25	0.085	43
rac-EBIZrX$_2$	0	0.046	32
rac-EBIZrX$_2$	20	0.092	13
rac-EBIZrX$_2$	50	0.064	10
rac-EBIZrX$_2$	50	0.034	18
rac-EBIHfX$_2$	50	0.030	32
rac-iPrBIZrX$_2$	50	0.038	52

the behavior of *rac*-EBIZrCl$_2$, *rac*-EBIHfCl$_2$, and *rac*-iPrBIZrCl$_2$, attempting to uncover quantitative details on dynamic processes that may help in the rational design of new catalysts.[4,5] For this, we decided to employ a joint experimental−theoretical approach and investigated metallocenium ion pairs (IPs) relevant to the polymerization behavior of the aforementioned catalytic systems in ethene−styrene copolymerization. In this respect, IPs afford both practical and theoretical advantages, as they are well-defined species that adequately represent the catalytically active species produced by activating the chloro complexes with MAO and are easily and cleanly obtained by reacting the metallocene precursors with a strong Lewis acid. It is worth noting that the counterion derived from tris(pentafluorophenyl)borane seems to be slightly less coordinating in nature than that obtained by employing MAO as cocatalyst.[6−9] One should thus expect any electronic effect extracted using the latter species to be somewhat intensified with respect to the former, which would, therefore, represent a useful proxy.

As for the dynamic processes of interest, it is noted that the catalytic pathway during olefin polymerization in the presence of metallocenes of group 4 is thought to involve the displacement of a coordinating anion from the metallocenium cation, which then enters into a catalytic cycle by repeated olefin uptake and insertion, leading to the formation of the growing chain.[6,10−12] (Chart 1)

Chart 1
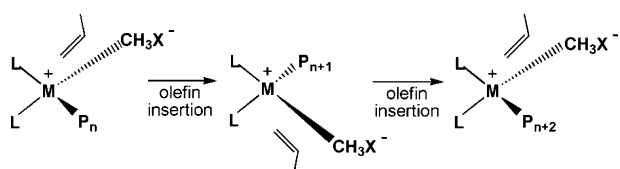
From the schematic mechanism of polymerization in Chart 1 it is intuitive that the IP strength ought to be strictly associated to the catalysts' polymerization performances,[6,13] at least because it controls the rate of olefin coordination. The IP

strength is related to the energy required to activate whole anion coordination site exchange, a process that can thus be used to gauge the acidity of the complex in a given solvent. Similarly, IP formation enthalpy (or the equivalent cocatalyst dissociation enthalpy) is also indicative of complex acidity and steric hindrance around the metal center, both modulated by the choice of ligand sphere. As a matter of fact, IP strength and formation enthalpy are closely related.[4]

In this work, the metallocene IPs *rac*-EBIZrMe—MeB-(C$_6$F$_5$)$_3$, **1**, *rac*-EBIHfMe—MeB(C$_6$F$_5$)$_3$ **2**, and *rac*-iPr-BIZrMe—MeB(C$_6$F$_5$)$_3$ **3** have been synthesized and their structures and aggregation states in solution explored by ROESY-NMR and pulsed gradient spectroscopy. The kinetics and energetics of dynamic processes in these IPs have also been studied by variable-temperature NMR experiments, with the hope of extracting useful data. Theoretical calculations were also employed to gauge the acidity of the metal centers. These combined results have brought to light the intricate way the metal and ancillary ligands influence the relative energetics of the IPs, their interaction with ethene and styrene, and consequently the reaction energy profile for the olefin coordination and insertion steps obtained with DFT calculations.

■ RESULTS AND DISCUSSION

This section is divided into two parts, the first of which describes experimental results on the aforementioned species, providing fundamental pieces of information on systems **1**−**3** relevant to our goal. Peculiarities in the dynamic behavior of **1**, which emerged while analyzing the data and which spurred us to supplement experiments with computations, are also discussed. In the second part, theoretical results on IP formation and other pertinent processes are presented and employed to discuss structural and electronic effects linked to changes in an IP metal and ligand sphere. Reaction energy profiles are subsequently analyzed on the basis of all pieces of information provided.

Experiments. The three IPs active in the ethene−styrene copolymerization, [*rac*-EBIZrMe]$^+$[MeB(C$_6$F$_5$)$_3$]$^-$ **1**, [*rac*-EBIHfMe]$^+$[MeB(C$_6$F$_5$)$_3$]$^-$ **2**, and [*rac*-iPrBIZrMe]$^+$[MeB-(C$_6$F$_5$)$_3$]$^-$ **3**, have been synthesized according to the literature. They differ respectively in the nature of the metal center and the ancillary ligands, with the anionic part of the systems being deliberately kept constant to limit the number of variables at play (Chart 2).

1. Ion Pair Structures in Solution. As a preliminary step in our investigation, we carried out pulsed gradient spin echo NMR (PGSE-NMR) measurements on systems **1** and **3** to evaluate the possible insurgence of aggregates that could misrepresent the kinetic processes of the IPs under investigation and possibly have a bearing on the catalytic
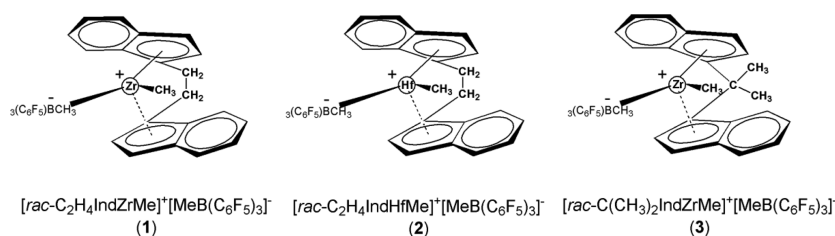
Chart 2

[*rac*-C$_2$H$_4$IndZrMe]$^+$[MeB(C$_6$F$_5$)$_3$]$^-$
(1)

[*rac*-C$_2$H$_4$IndHfMe]$^+$[MeB(C$_6$F$_5$)$_3$]$^-$
(2)

[*rac*-C(CH$_3$)$_2$IndZrMe]$^+$[MeB(C$_6$F$_5$)$_3$]$^-$
(3)

Table 2. Diffusion Coefficient D_t, Hydrodynamic Radius r_H, Hydrodynamic Volume V_H, and Aggregation Number N for Systems 1 and 3 at Concentration C

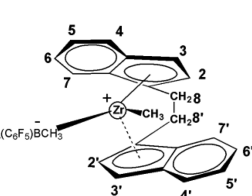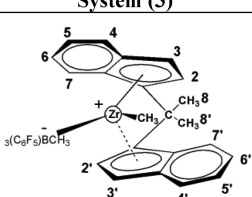| system	C (mol L^{-1})	D_t (m^2 s^{-1})	r_H (Å)	V_H (Å^3)	r_{vdw} (Å)	V_{vdw} (Å^3)	N (V_H/V_{vdw})
[*rac*-EBIZrMe]$^+$[MeB(C$_6$F$_5$)$_3$]$^-$	0.01	7.18×10^{-10}	5.65	755	5.25	607	1.2
[*rac*-iPrBIZrMe]$^+$[MeB(C$_6$F$_5$)$_3$]$^-$	0.01	7.05×10^{-10}	5.75	796	5.28	616	1.3

activity. Table 2 shows the results for the hydrodynamic and van der Waals volumes obtained by these experiments (see the Experimental Section).

The ratio $N = V_H/V_{vdW}$ gives an indication of the relative size of the systems that describes their diffusion with respect to the bare van der Waals excluded volume. In principle, N should be expected to be slightly larger than unity due to both the viscous drag and the non-hard-sphere type molecular boundaries. From the data it appears that there was no detectable aggregation in a 0.01 M solution in benzene as one could expect for inner-sphere ion pairs (ISIPs);[14] consequently, the remaining NMR experiments were carried out at this molar concentration, which is higher than the concentration generally used during ethene–styrene copolymerization (0.18–0.28 mM). Table 2 thus gives an indication that no aggregated active species should be involved during such a process.

Systems **1** and **3**, which are expected to present the greatest structural differences, were also characterized in deuterated benzene (C$_6$D$_6$) using quantitative ROESY-NMR techniques to acquire IPs structural details. These may be useful in discussing the catalytic behavior during ethene–styrene copolymerization. A single reference hydrogen–hydrogen (H$_2$–H$_3$) distance for each species was used to set the absolute length scale; such a distance was obtained from the gas-phase DFT optimized structure of the dichloro precursors, whose geometries are expected to be robust with respect to the level of theoretical treatment. Table 3 provides a comparison between distances (other than that used for calibration) in the precursors and IPs estimated by ROESY-NMR and by theoretical modeling.

As one can see, gas-phase DFT distances are consistent with the experimental values extracted from solution measurements. Larger differences can be seen for a few aromatic protons (e.g., H$_5$–H$_7$ in system **1** and H$_{4'}$-H$_{5'}$ in system **2**) that should present rigid bonds and highly reproducible distances. This apparent incongruence can be ascribed to the presence of

Table 3. Hydrogen–Hydrogen Experimental and Theoretical Distances Obtained for Systems 1 and 3

System (1)	distance	d_{exp} (Å)	d_{teor} (Å)	Δd_{teor_exp} (Å)
	ZrCH$_3$-H$_2$	3.42	3.63	0.21
	ZrCH$_3$-H$_{3'}$	4.05	4.42	0.37
	BCH$_3$-H$_{3'}$	3.81	3.35	-0.46
	H$_5$-H$_7$	4.93	4.35	-0.58
	H$_8$-H$_2$	3.72	3.63	-0.09
	H$_{8'}$-H$_{2'}$	3.30	3.37	0.07
	H$_8$-H$_7$	2.77	3.06	0.29
System (3)				
	ZrCH$_3$-H$_2$	3.41	3.44	0.03
	ZrCH$_3$-H$_3$	2.96	3.24	0.28
	BCH$_3$-H$_{3'}$	3.26	3.50	0.24
	H$_{2'}$-H$_{3'}$	2.73	2.67	-0.06
	H$_{4'}$-H$_{5'}$	2.79	3.17	0.38
	H$_8$-H$_2$	2.61	2.89	0.28
	H$_{8'}$-H$_{2'}$	2.75	2.87	0.12
	H$_8$-H$_7$	2.62	2.69	0.07

particularly crowded NMR aromatic regions (Figure S6, Supporting Information), with a possible partial signal overlapping and non sharply defined peak integration ranges. The IP formation, in fact, induces the precursor desymmetrization, thus doubling the amount of aromatic NMR signals with respect to the precursor. More in general, slightly larger deviations are seen for **1**; these could be due to a higher conformational flexibility of such an IP in solution (vide infra). An additional test of DFT performance was carried out by constraining interatomic distances to the available experimental values and reoptimizing the IPs' structures. The latter presented only minor differences from the unconstrained counterparts in terms of both energy and geometrical values, thus supporting the idea that the geometries of ISIPs are well described by gas-phase DFT calculations and validating the possibility of extracting more complex details, such as geometrical parameters, from theoretical modeling (Chart 3 and Table 4).

With respect to catalytic performances, the graphical representation of the indenyl–metal part of IPs in Chart 3

Chart 3
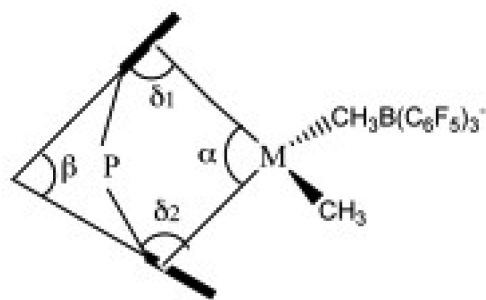
shows that angles α and β give indications of the metal center encumbrance due to the indenyl moieties; in fact, by increasing α and diminishing β the metal becomes more "sunken" into the Cp system. DFT-based data in Table 4 show that complex **1** has higher α and lower β values; i.e., it has a more hindered metal center with respect to **3**. As hinted at in the Introduction, a similar indication emerged from the precursor X-ray structures and was used to justify the lower reactivity toward the "bulkier" styrene during olefin enchainment driven by the ethylene-bridged systems, an argument that appears to us insufficient on its own. Thus, we decided to study experimentally the solution dynamics of the IPs in order to explore further the differences in behavior for **1**–**3**, attempting to correlate such a dynamics with that involved during the polymerization process (e.g., in the monomer coordination–insertion).

1. Ion Pair Electronic Properties: Dynamic Processes in Solution. As briefly discussed in the Introduction, energetic data on dynamic processes directly connected with IP electronic properties would be useful to shed additional light on the different catalytic properties of systems **1**–**3**. In fact, polymerization of alkenes catalyzed by metallocenium IPs can be summarized in the following steps: (a) displacement of the

Table 4. Structural Details (in deg) of the Indenyl−Metal Part of the Precursor and IP for the Three Species Investigated in This Work[a]

geometrical param	system 1 (exp)	precursor 1 (exp)	precurson 1 (RX)	system 3 (exp)	precursor 3 (exp)	precursor 3 (RX)
α	125.8	125.4	126.9	117.6	116.4	118.1
β	62.2	61.9	62.1	73.9	73.4	70.9
δ_1	83.6	84.9	84.6	83.2	83.4	85.0
δ_2	85.1	84.1	84.6	82.8	83.4	85.0

[a]RX indicates X-ray diffraction results and refers to the neutral precursor, while the results denoted exp were obtained with gas-phase DFT optimizations of the IP and precursor structures constraining a few interatomic distances to available experimental distances (see the Experimental Section for details).

Chart 4

borane exchange   anion exchange

chain growth
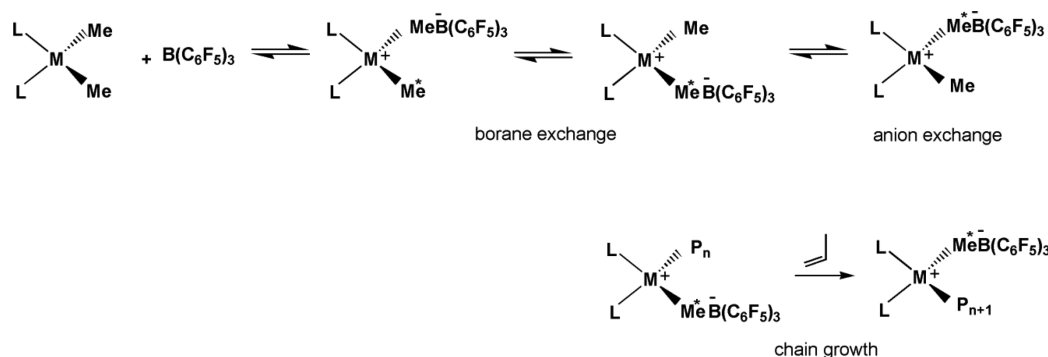
anion from one of the two positions around the cation (the other being occupied by the growing chain) during monomer coordination, (b) migratory chain transfer to the β-carbon of the coordinated monomer, and (c) reassociation of the anion into the catalytic site previously occupied by the alkyl chain. Then, a key question in understanding the performance of metallocenium-based catalysts relates to the energy required for the anion displacement and the contemporary or subsequent monomer coordination. In absence of monomers, an IP in solution presents at least two kinetic processes that can provide indication of the energetics involved in the polymerization processes: (i) the anion exchange and (ii) the cocatalyst (borane) exchange (see Chart 4) as discussed above. However, anion exchange is more fundamental in nature, as discussed in the following.

Variable-temperature 1-D ^{1}H NMR experiments allowed us to evaluate the relative rates of those two processes,[4,15] since the broadening of methide (M-Me) and aromatic Cp signals can be used to determine their rate by means of the equation $k = \pi(\Delta W)$. Here, k is the rate constant in s^{-1}, $\Delta W = W_2 - W_1$, W_2 is the line width at half-height of an exchange-broadened peak in Hz, and W_1 is the line width at half-height in the absence of exchange in Hz.[16]

NMR line widths of methide (M-Me) and aromatic (H-Cp) signals in the range from −20 to +70 °C are reported in Table 5.

We begin our discussion on these data by mentioning that $\mathbf{1}$[13,15] and $\mathbf{2}$[15] have been previously studied with variable-temperature NMR, albeit covering a narrower (and higher) range of temperatures than in Table 5; $\mathbf{3}$ is investigated here for the first time with the same approach, as far as we know. However, a similar IP bearing a $(CH_3)_2Si$ bridge instead than $(CH_3)_2C$ has been studied previously.[17] From Table 5, it emerges that $\mathbf{3}$ shows a monotonic increase in line width for temperatures above 10 °C, as one would expect. Conversely, the line widths for $\mathbf{1}$ and $\mathbf{2}$ present a very odd behavior: for

Table 5. ^{1}H NMR Line Width of Methide (M-Me) and Aromatic (H-Cp) Signals in the Range from −20 to 70 °C for Systems 1−3

T (°C)	system 3 $W_{\text{M-Me}}$	$W_{\text{H-Cp}}$	system 1 $W_{\text{M-Me}}$	$W_{\text{H-Cp}}$	system 2 $W_{\text{M-Me}}$	$W_{\text{H-Cp}}$
−20	n.d.	n.d.	2.13	5.17	4.20	7.17
−10	2.38	5.72	2.31	5.65	4.20	7.34
0	2.32	5.88	2.66	6.30	3.24	6.38
10	2.48	5.84	3.09	7.17	3.44	5.68
20	3.00	6.41	1.66	4.96	4.20	5.59
30	3.59	6.98	1.67	5.23	5.53	5.07
40	3.76	7.54	1.93	5.88	11.45	6.29
50	4.61	8.17	2.25	6.11	n.d.	6.90
60	5.55	9.01	3.07	6.75	n.d.	n.d.
70	7.35	10.21	5.88	8.97	n.d.	n.d.

system $\mathbf{1}$, W increases in the interval −10 to +10 °C, it suddenly decreases around 20−30 °C, and it increases again, albeit in a less marked fashion, upon increasing T above 30 °C. For system $\mathbf{2}$, the W trend is similar, even though the variations are less marked.

At variance with the monotonic temperature dependence expected for W in $\mathbf{1}$ and $\mathbf{2}$, the experimental data seem to indicate the presence of, at least, another dynamic process in addition to anion exchange and borane migration. We note that such a process ought to be fast already at low temperature and, also, that it becomes less able to influence the line width above 20 °C. In this respect, the peculiarities of our experimental data at low temperature direct us toward the possibility of interconversion between the indenyl-forward (Π) and the indenyl-backward (Y) conformations (Chart 5) for the cationic part of $\mathbf{1}$ put forward by Piemontesi et al.[18] for the precursor rac-EBIZrCl$_2$. Indeed, they reported the presence of such two conformations in solution, suggesting Π as the more stable and, consequently, predominant conformation at low temperatures.

Chart 5

Π conformation
(indenyl-forward)

Y conformation
(indenyl-backward)
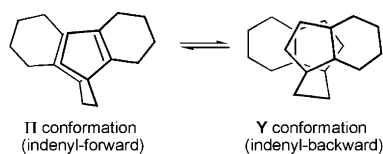
To examine the possibility of having present species with marked structural differences, we performed ^{19}F NMR experiments, as the difference in chemical shifts between *meta* and *para* fluorines, $\Delta\delta_{m,p\text{-}F}$, gives information on the possible presence of differently coordinated species: the larger the $\Delta\delta_{m,p\text{-}F}$ value (in the range 3–6 ppm), the more tightly coordinated the anion.[19] The ^{19}F NMR spectrum of [*rac*-EBIZrMe]$^+$[MeB(C_5F_6)]$^-$ reported in Figure 1a shows the
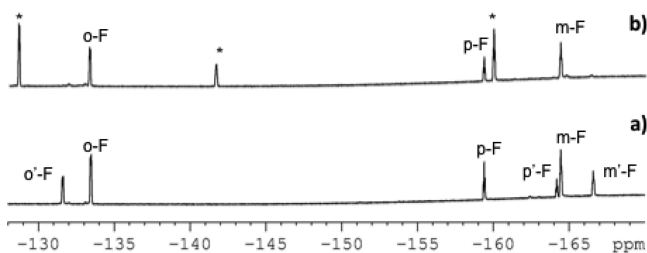

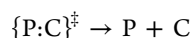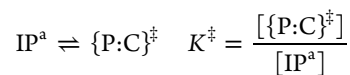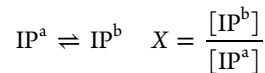**Figure 1.** ^{19}F NMR spectra of system **1** (a) and system **3** (b) at 20 °C in toluene-d_8 (400 MHz). Asterisks indicate the unreacted B(C_6F_5)$_3$.

presence of two patterns of signals for [MeB(C_5F_6)]$^-$, both ascribable only to μ-Me coordinated species. Conversely, no indication is found for noncoordinated anions ($\Delta\delta_{m,p\text{-}F}$ < 3 ppm). The ^{19}F NMR data thus support the hypothesis of a fast Π–Y interconversion. Unfortunately, a similar analysis of **2** could not be carried out, due to its lower purity.

A more detailed scrutiny of the Π–Y conformational flexibility of ethylene-bridged species was carried out with DFT relaxed scans to evaluate relative energies and interconversion barriers. These were conducted by driving the torsional angle between the planes defined by the four carbon atoms involved in the ring tethering: one on each cyclopentadienyl ring and the two belonging to the CH_2CH_2 bridge. As for the Zr-containing species, we found that the dimethyl precursor presents two conformers of the same type shown in Chart 5, with the Π conformation being roughly 1.3 kcal/mol more stable than the Y form; **1** presents two degenerate conformers, the Y species being 0.01 kcal/mol more stable than the other. A scan along the dihedral angle also indicated the presence of a barrier of roughly 3.1 kcal/mol on going from the Π conformer toward the Y species in both cases. A similar situation is also found for the Hf-containing species, the only differences being a marginally more stable Y precursor (only 1.1 kcal/mol higher than Π) and a lower interconversion barrier (2.9 kcal/mol). Thus, the energetics results, together with the ^{19}F NMR spectra, clearly support both the presence of two conformers at all temperatures investigated and their fast interconversion, a dynamic process that is expected to have an important bearing on the interpretation of the NMR results, due to the difficulty in defining line widths in the absence of exchange as hinted above. Also, they indicate that the bulky nature of the counteranion influences the relative Π–Y stability, making the two conformations possible for **1** and **2** isoenergetic.

The presence of low-energy dynamic processes introduces additional complications other than the definition of a reference line width. To show that this may be the case, let us consider the borane retrodissociation process, an example for which one needs to take into account the flexible nature of the ethylene-bridged IPs that must be described using, at least, the following simplified mechanistic model:

$$IP^a \rightleftharpoons IP^b \quad X = \frac{[IP^b]}{[IP^a]}$$

$$IP^a \rightleftharpoons \{P{:}C\}^\ddagger \quad K^\ddagger = \frac{[\{P{:}C\}^\ddagger]}{[IP^a]}$$

$$\{P{:}C\}^\ddagger \rightarrow P + C$$

with P:C‡ being the activated complex of transition state theory in the Eyring form. In this case, the effective rate for the dissociation of the total concentration of IP into P (precursor) and C (cocatalyst) is proportional to $K^\ddagger/(1 + X)$, with both the ^{19}F NMR spectra and our DFT calculations suggesting $X \approx 1$. In this case, the effective rate constant (or its counterpart multiplied by $1/T$ in an Eyring plot) will not follow a simple exponential behavior with respect to $1/T$[20] due to the presence of two overlapping trends. This peculiar situation, in our view, makes difficult any further consideration on the IP kinetic processes in **1** and **2** by variable-temperature NMR experiments.

Turning back to **3**, the presence of a single species in the ^{19}F NMR spectrum of this system (Figure 1b) and the monotonic behavior of the line width with respect to T appears well justified by the different structure of *rac*-iPrBIZrMe$^+$, the latter characterized by the presence of a single carbon atom bridge that effectively divaricates the "pocket" occupied by the metal and heavily restricts the torsional motion of the indenyl moieties. The correct behavior of the line width, a plateau at low temperature followed by a monotonic increase upon increasing T, allows us to estimate rate constants as $k = \pi\Delta W$. In this case, an exchange rate constant of roughly 3.5 s^{-1} at 30 °C is obtained using the data from both the zirconium-bound methyl group Me-M and the H-Cp protons on the cyclopendadienyl rings; this value is found to be in good accordance with what is obtained for the similar (CH_3)$_2$Si-bridged complex (4 ± 0.8 s^{-1} at 25 °C).[17] Arrhenius and Eyring plots for the rate constants computed using the W data in Table 5 for **3** suggest that the dynamic process requires 8–10 kcal/mol to be activated, a value substantially smaller than what was estimated previously for a large set of IPs in nonpolar solvents[4,15] for both anion exchange and borane migration. With published data suggesting that no barrier should be expected for the borane retrodissociation[4] and IP formation enthalpies usually of the order of 17–21 kcal/mol for similar species, our finding might be taken as indicating the presence of a less energetically demanding dynamic process. At the moment, it seems difficult to propose any sensible process on the basis of the available data. Nevertheless, we mention in passing as possible the IP isomerization that substitutes the μ-Me coordination of the anion on the metal center with an interaction of the latter with a *o*-fluorine on the counterion.[21] For this species, we estimated a gas-phase energy difference of roughly 7 kcal/mol, which is expected to decrease in solution due to charge-screening effects.[21]

In summary, the experimental data indicate that the investigated IPs are monomeric species at the concentrations of interest and have solution structures characterized by a metal center coordinated to the anion via μ-Me bond and seemingly well described by gas-phase DFT calculations and suggest the presence of, at least, an additional dynamic process (Π–Y isomerization for ethylene-bridged species and, possibly, the formation of a species with an F-coordinated instead than μ-Me-coordinated anion) for all species in addition to those of direct importance to the energetics of ethene–styrene copolymerization. To explore the latter, we are thus forced to employ theoretical means, the results of our DFT calculations being described next.

2. Influence of the Ion Pair Strength on the Coordination and Insertion Barriers of Styrene vs Ethene: Acidity Gauges. As indicated above, IP strength can be used to directly gauge the acidity of the cationic moiety, as the same counteranion is present in **1**–**3**. In fact, one would expect that the more acidic the cation, the higher the energy required to detach the two ions.

Although it is in principle possible to compute directly the energy difference between an IP and its dissociated counterions,[22] it is technically more robust to estimate the variation of this quantity by employing the reaction:[23]

$$C_i^+ A^- + C_j^+ \rightarrow C_i^+ + C_j^+ A^- \quad \Delta\Delta E_{IP}(j, i)$$
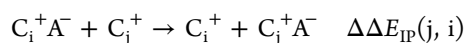
where C_i^+ represents one of the cationic moieties, A^- is the counteranion, $\Delta\Delta E_{IP}(j,i) = \Delta E_{IP}(j) - \Delta E_{IP}(i)$ is the anion exchange energy, and $\Delta E_{IP}(i)$ is the energy released forming the IP with the C_i^+ cationic group from the oppositely charged dissociated fragments. Using this isodesmic approach, one avoids treating the problematic anion in isolation; since pulsed gradient NMR results suggest IPs do not aggregate in quadruplets or larger clusters, we are allowed to avoid a more demanding level of modeling while treating anion exchange.

Table 6 gives the results obtained using gas-phase DFT calculations and the cation $[rac\text{-EBIZrMe}]^+$ as a reference C_i^+. The latter cation was employed as reference due to its lower relative reactivity with respect to styrene under all conditions.

From the results in Table 6 it emerges that the IP containing $[rac\text{-EBIZrMe}]^+$ is indeed the least strongly bound, suggesting a

Table 6. Anion Exchange Energy (in kcal/mol) with Respect to $[rac\text{-EBIZrMe}]^+$ as $C_i^{+\ a}$

Exchange process		C_i^+	C_j^+	$\Delta\Delta E_{IP}$
		EBIZr	EBIHf	+1.4
		EBIZr	iPrBIZr	+3.1

[a] Cations C_i^+ are indicated as YM, with Y and M representing the bridging moiety and aromatic ligands (i.e. EBI or iPBI) and the metal atom (Zr or Hf), respectively.

lower acidity of this cation moiety when this is gauged by anion exchange. Substituting Zr with Hf or divaricating the ligand pocket by tethering the indenyl groups with a single carbon atom bridge produces more stable IPs, thus suggesting a stronger acid character for the last two species. Comparing directly $[rac\text{-EBIHfMe}]^+$ and $[rac\text{-iPrBIZrMe}]^+$, however, is hampered by the fact that there are two key chemical differences between them, a fact that suggests exploring alternative measures for the cation acidity to be worthwhile. Thus, we opted for investigating also the energetics of exchange reactions transferring either the methide anion or an olefin (ethene and styrene) between two cationic moieties due to their relevance to the polymerization. Tables 7 and 8 provide such results.

Table 7. Methide Exchange Energy (ΔE_{MeEx}, in kcal/mol) with Respect to $[rac\text{-EBIZrMe}]^+$ as $C_i^{+\ a}$

Exchange process		C_i^+	C_j^+	ΔE_{MeEx}
		EBIZr	EBIHf	+5.4
		EBIZr	iPBIZr	+1.9

[a] Cations are labeled as indicated in Table 6.

Table 8. Ethene/Styrene Exchange Energy (in kcal/mol) with Respect to $[rac\text{-EBIZrMe}]^+$ as $C_i^{+\ a}$

Exchange process (ethene)		C_i^+	C_j^+	ΔE_{EtEx}
		EBIZr	EBIHf	+1.1 (+1.7)
		EBIZr	iPBIZr	+1.8 (+2.7)

[a] Data for styrene are given in parentheses. Cations are labeled as indicated in Table 6.

From the data in Table 8, one notes that olefin exchange provides an acidity scale that agrees well with what was found previously for the anion. Instead, the data provided for the methide anion exchange (Table 7) suggest the dimethyl precursor of **2** to be 3.5 kcal/mol more stable than that of **3**.

In principle, the difference between the three acidity scales may be reconciled by assuming the methide exchange to be a more direct measure of electronic acidity, due to the smaller size of the exchanged anion; a reduced strain should thus be needed to adapt a ligand pocket in order to accept the latter. In other words, a direct comparison of relative stabilities for species that bear different bridges should factor in that *rac*-EBI-derived species may be in favor of "less crowding" when it come

to bulky ligands,[24] a bias that ought to play a lesser role in case of Me⁻ abstraction. While one may thus feel reasonably confident in assigning a global lower acidity to the cation in **1**, defining the relative acidity of **2** and **3** requires further development of our analysis.

To do so, we note that exchange processes can be decomposed further as a sum of two steps for each cation: first, a ligand detachment formally maintaining the cation with the same optimal geometry in the presence of the ligand, and second, a subsequent structural relaxation to the cation minimum geometry. In this way, one hopes to isolate better the electronic component of the exchange (and hence of the dissociation) processes from the related geometrical stress. In fact, it would be enough to evaluate the cation relaxation energy, $\Delta E(L)_{Relax}$, for such a comparison, as this is a measure of how strongly the ligand is "drawn" into the cation coordination sphere, displacing the other ligands from their optimal positions. Table 9 gives the results for $\Delta E(L)_{Relax}$, where L = Me⁻, methyl borate anion, ethane, styrene represents the ligands.

Table 9. Relaxation Energy ($\Delta E(L)_{Relax}$, in kcal/mol) for the Three Cations Derived from 1–3[a]

cation/ligand	L = Me⁻	L = anion	L = ethene (styrene)
[*rac*-EBIZrMe]⁺	−5.39	−3.80	−2.40 (−2.49)
[*rac*-EBIHfMe]⁺	−7.70	−5.93	−3.80 (−4.11)
[*rac*-iPrBIZrMe]⁺	−4.42	−2.04	−1.56 (−1.75)

[a]The initial structure is identical with that in the complex with ligand L; the equilibrium geometry for the free cation was used as the final structure.

On the whole, the comparison among data shown in Tables 6–9 indicates clearly that the Hf-containing species is the most acidic from an electronic standpoint, being capable of the strongest "pulling" of any of the studied ligands into its coordination sphere. The latter effect fully justifies the differences between cations derived from **1** and **2**, especially in view of the weak structural changes upon substituting Zr with Hf in both the free cations and neutral precursors. Note also that the apparently higher acidity of [*rac*-iPrBIZrMe]⁺ with respect to [*rac*-EBIZrMe]⁺ shown in Tables 6–8 is not completely justified by the wider "pocket" geometry in the former, which affords it a reduced geometrical strain. Electronic factors are thus playing a role as well, so that we feel justified in indicating a more acidic nature for the metal cation in **3** than in **1**.

To conclude our discussion on possible acidity gauges for the cationic moieties in **1–3**, we recall that among the quantities amenable to experimental investigation there is also the energy ΔE_{Form} (or enthalpy ΔH_{Form}) of IP formation from the neutral dimethyl precursor complex and the trialkylborane. In fact, this should be the most easily accessible quantity via direct calorimetric titration or, indirectly, via dynamic NMR measurements.[4] However, its interpretation in terms of chemical and structural details of the IP is not necessarily straightforward.[13] Since ΔE_{Form} is also amenable to theoretical exploration via electronic structure methods both in the gas-phase and with implicit model solvents,[21,22,24–26] we nevertheless estimated it for **1–3**. This was done with the aim of shedding additional light on the role played by the metal center and ligand sphere in defining this important quantity and, hopefully, drawing a clearer connection between this nontrivial quantity and the

cation acidity. Table 10 contains the results obtained with our modeling method.

Table 10. Gas-Phase Formation Energy ΔE_{Form} for an IP from the Neutral Complex Precursor and the Trialkylborane (in kcal/mol)

formed species	ΔE_{Form} (kcal/mol)
1	−15.9
2	−11.9
3	−17.1

As expected, the formation energies are substantially negative, thus indicating a stabilization of the IPs even in the gas-phase due to Coulomb interaction between the μ-coordinated methyl on the anion and the metal center; they are also in line with what is found for simpler bis-cyclopentadienyl Zr complexes.[24] It seems, however, that the larger indenyl-based ligand exerts some effect on the energetics of the IP formation, reducing the energy release with respect to the latter species. Slightly more negative values should be expected for the same process in solution,[24] thanks to the stabilization of the IP due to solvent polarization.

From the data in Table 10, one clearly notes the stark electronic effect of metal substitution, with **2** releasing the lowest amount of energy upon formation. The effect of varying the metal center on IP formation was previously highlighted in the literature, both theoretically[24] and experimentally,[4,15] as it may have important consequences on the chemistry of homogeneous catalysts (see refs 3, 27, and 28 and references therein). Finally, a weaker effect is also present as a function of the different bridges between the indenyl moieties. As for the latter, the discussion provided regarding IP strength should have made it clear that changes in the geometry of the coordination sphere induced by different bridges might transfer into non-negligible electronic effects.

Bearing in mind the data in Tables 6–9, the effect of cation acidity on ΔE_{Form} (or the related enthalpy) can be conveniently investigated by decomposing the formation process as indicated in Chart 6, the two key processes in it (i.e., methide abstraction and etherolytic IP dissociation) being amenable also to experimental investigation.[4]

Chart 6
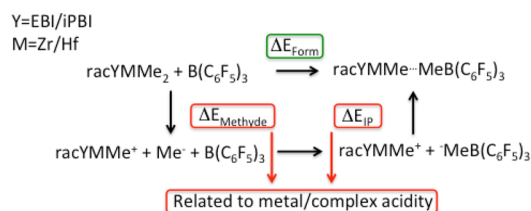
From Chart 6, it emerges that acidity effects would partially cancel in the overall process, a fact that introduces the source of difficulty in interpreting quantitative results on ΔE_{Form} hinted above. In our case, however, the results in Tables 6–8 clearly indicate that the substantial difference in ΔE_{Form} between **1** and **2** is due to a higher energetic requirement for the heterolytic dissociation of the Hf−Me bond than for the Zr−Me bond, whereas the additional stability afforded by the anion in binding to [*rac*-EBIHfMe]⁺ represents only a minor energetic effect. As for the comparison between **1** and **3**, our data indicate that the

more negative value of ΔE_{Form} for **3** emerges from a more stable IP, which overcompensates for the higher methide abstraction energy. Thus, it seems that the wider pocket afforded by **3** is of fundamental importance in defining the overall behavior of the latter with respect to a donating ligand; electronic effects induced by the more obtuse angle between indenyl moieties cannot, however, be neglected.

Reaction Profiles. The data on the relative acidity and steric encumbrance are helpful in rationalizing the different behaviors in terms of the fraction of styrene inserted during the copolymerization catalyzed by the cations in **1**−**3**. In fact, they represent key pieces of information when it comes to interpreting the differences in the energy profiles followed by the olefins to, first, coordinate to and successively propagate the chain onto the metal center. Results obtained for the very first step of the polymerization, i.e. with the methyl group bound to the metal instead of a more customary C_2 (or C_{2n}) chain, are provided in Figure 2. The stationary points optimized during
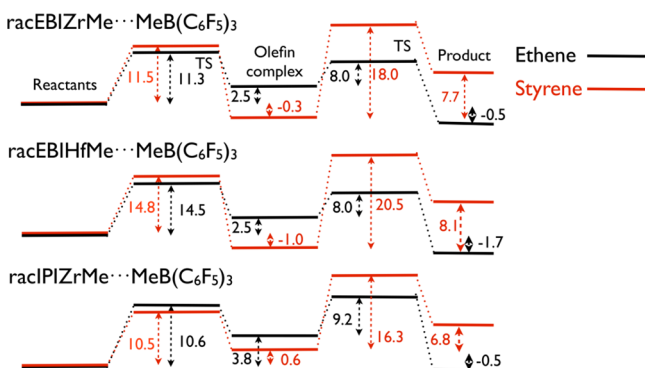

Figure 2. Energy profile for the olefin coordination onto the metal center and insertion into the M−Me bond of the IPs studied with respect to the reactants (ion pair plus olefin). Energies are given in kcal/mol.

the calculations on the Hf-bearing species are shown in Figure 3. These are representative of the general structural characteristics also for species derived from **1** and **3**.

There are qualitative differences between ethene and styrene, as well as between species having different bridges. It appears that the intermediate ethene−ion pair complexes always lie higher in energy (at least 2.5 kcal/mol) than the reactants as previously found,[24,29] whereas the equivalent species with styrene are more stable or marginally less stable (0.6 kcal/mol, **3**) than the reactants (**1** and **2**). Moreover, there is a substantially lower TS barrier for the insertion of ethene onto the M−Me bond than for styrene, so that enchaining ethene requires less energy than retrodissociating it from its complexes with **1** and **2**. The TS barrier for styrene enchainment is instead always higher than that for the retrodissociation, a finding also present for the ethene enchainment catalyzed by **3**. Finally, we mention that relaxing a structure right after having surmounted the chain propagation TS leads to products with a non-coordinated counterion, effectively locked out from the coordination sphere of the metal by the growing chain bound to the latter via a γ-agostic interaction. Despite this, the postenchainment minima involving ethene are lower in energy than those of the reactants; the opposite is instead true for styrene. The latter difference in results seems to be related to the dissimilar steric encumbrances of the two olefins, the chain
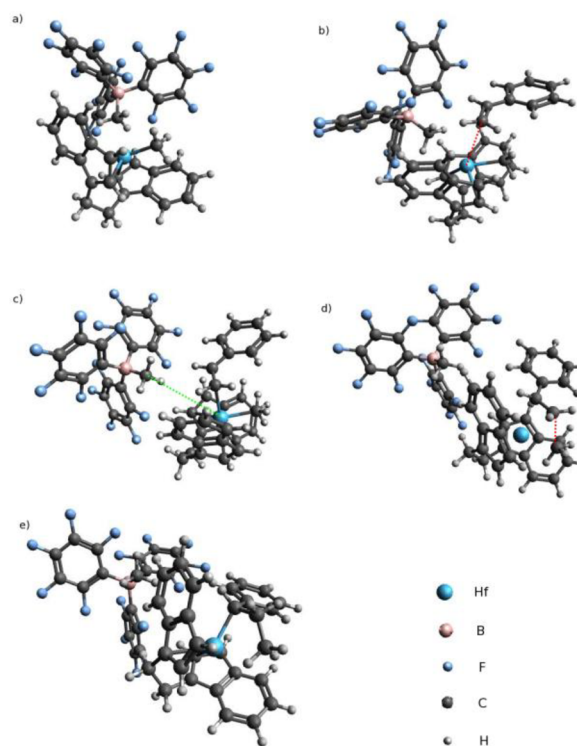

Figure 3. Stationary point geometries for the IP **2** (a), its styrene complex (c), styrene coordination (b) and insertion (d) transition states, and enchainment product (e). Note the secondary insertion geometry found for styrene. Red dashed lines represent TS search reaction coordinates.

containing styrene forcing the counterion to stay farther away from the metal center.

Given the bulkier nature of styrene, the increased stability of styrene complexes with respect to the reactants in comparison to ethene complexes can only be justified by electronic effects, the aromatic substituted olefin being more prone to donate the electrons in the π cloud of the double bond. In fact, the most acidic cation according to our discussion (vide supra) produces a relatively more stable styrene complex, thus suggesting that it is the energy associated with the π coordination that plays the most important role after the expulsion of the counteranion from the first coordination shell. Noting that all olefin coordination TS's present an anion still μ-coordinated via the Me group to the metal (see Figure 3 and the Supporting Information), it becomes evident that acidity also rationalizes the relative heights of the coordination barriers in **1** and **2**, as it is the relative strength of the μ-coordination bond that plays the key role in defining the latter quantity. The wider "pocket" present in **3**, instead, somewhat masks the acidity effect, reducing the strain induced by the incoming olefin and allowing the latter to come closer to the metal center.

The higher energetic requirements for styrene than for ethene in the propagation step is not surprising in lieu of the stabilization of the intermediate complex, as well of the inductive and conjugative effects of aromatic substituted olefins.[30] The net effect of such characteristics for styrene on its reaction profiles is the pre-equilibrium nature of all its intermediates, which is at variance with what is found for ethene when enchained by **1** and **2**. In the latter cases, the low energetic requirement for the propagation step favors it with

respect to the ethene retrodissociation from the complex, as also indicated in ref 29.

Interestingly, Oliva et al.[1] have already hypothesized the kinetic bottleneck for the overall polymerization process to be the olefin coordination for ethene and the enchainment step for styrene. Despite the additional data in ref 27, such an hypothesis has been only indirectly supported by the theoretical modeling in ref 31, where a higher insertion barrier for styrene than for ethene was obtained using the bare cation as catalyst. However, it is only with the inclusion of the counteranion in the catalyst model, and the consequent possibility of estimating retrodissociation barriers, that one can justify on robust grounds the temperature dependence of the ethene–styrene composition extracted experimentally for **1** (Table 1). Specifically, the increasing fraction of styrene in the polymer upon decreasing the temperature is due to an increase in the concentration of the styrene–ion pair complex. Coupled with the, at least, 10-fold higher concentration of styrene in the feed, the higher stability of the styrene complex with respect to that of the ethene complex effectively limits the possibility for the lighter olefin to form the required intermediate (note also that the complexation barrier heights are quite similar).

The higher relative stability found for the styrene complex with **2** in comparison of that with **1** also helps rationalizing the fact that the former inserts a higher fraction of substituted olefin at 50 °C despite a higher insertion barrier (see Table 1). With the light olefin effectively excluded from forming the complex with the IP, **2** is only allowed to insert the substituted alkene. This happens despite the lower activity observed experimentally for **2**,[1] which is now a posteriori justified by the higher coordination barriers shown in Figure 2. Playing a role in boosting the tendency of **2** to insert more styrene than **1**, there is also the fact that the relative height between the styrene enchainment and retrodissociation barriers is lower for **2** (4.7 kcal/mol) than for **1** (6.2 kcal/mol); thus, the ratio between dissociation and insertion rate constants ought to be expected to be lower for the former. This difference is, again, a direct consequence of the more acidic behavior indicated for the Hf-based catalyst, the net effect on the reaction profile being to increase the height of the coordination TS more than the stability of the intermediate or the enchainment barrier.

The additional investment in computational time required by incorporating the anion pays off even more when dealing with **3**, as its reaction profile indicates that a pre-equilibrium should also be expected for the complex of ethene with the latter. In fact, we predict a lower barrier (by roughly 2.4 kcal/mol) for the ethene retrodissociation than for the insertion into the M–Me bond, at variance with what is found for **1** and **2**. In the case of **3**, the opposite order of barrier heights for the ethene complex suggests that the competition between light olefin enchainment and retrodissociation is in favor of the latter; thus, the total amount of ethene inserted by **3** ought to be lower than for **1** and **2**.

As a final piece of analysis based on our data, we highlight the fact that, apart from the importance in defining the energetic details of the competition between the two olefins and helping its rationalization, the presence of the methyl borate anion also has an impact on the relative stability of the olefin complexes with **3**. On one hand, it is in fact found (see Table 7) that exchanging either ethene or styrene between [*rac*-EBIZrMe]⁺ and [*rac*-EBIHfMe]⁺ or [*rac*-iPrBIHfMe]⁺ lowers the energy, the exchange between [*rac*-EBIZrMe]⁺ and [*rac*-iPrBIZrMe]⁺ being the most stabilizing (−1.8 and −2.7 kcal/mol,

respectively). On the other hand, exchanging an olefin between **1** and **3** appears to require energy (1.2 and 0.9 kcal/mol, respectively, for ethene and styrene), an effect that seems related to the slightly higher acidity and, hence, stronger μ-methyl interaction of the anion seen for **3** induced by its wider pocket. The loss of the μ-methyl interaction can be only partially compensated by the olefin during coordination, as the latter is less capable of satisfying the stronger electronic demand of [*rac*-iPrBIZrMe]⁺ with respect to [*rac*-EBIZrMe]⁺ than the anion itself. In our view, these last data stress even more the importance of including explicitly counterions for a detailed analysis of the energy profiles in Ziegler–Natta catalysis, their presence appearing to induce substantial modifications in the global energy landscape.

The same conclusions discussed above hold even for species in which the metal bears an ethyl group instead of a methyl group, as a qualitatively identical picture emerges from our results. In fact, the only difference worth mentioning with respect to the data in Figure 2 is a 3–5 kcal/mol reduction of the insertion barrier for the olefins into the metal–primary carbon bond (see the Supporting Information), an effect due to a β-hydrogen agostic interaction. The latter is slightly more marked for the Hf-based catalyst due to its higher acidity. No such effect is expected to be present at the coordination TS, as the presence of the bulky anion effectively blocks the reorientation of the alkyl group.

■ CONCLUSIONS

In this work, we employed a joint experimental–theoretical approach to investigate the properties of the IPs **1**–**3**, our aim being to rationalize their performances when involved in the Ziegler–Natta catalysis of ethene–styrene copolymers. While the experimental analysis helped to clarify the structure and aggregation state of the studied IPs, we encountered difficulties while trying to extract energetic details for processes such as anion site exchange and borane transfer. However, data from variable-temperature NMR seem to indicate that a complicate set of dynamic processes is active even at the lowest temperature explored.

By means of DFT calculations, we quantitatively investigated the role played by steric and electronic effects in defining the ion pair strengths and formation energies of **1**–**3**. Our computational data strongly support the view not only that hafnium should be considered a stronger Lewis acid than zirconium in this species but also that there are non-negligible electronic effects induced by a modification of the bridge between indenyl moieties. In particular, the isopropylidene bridge appears to induce a somewhat higher acid character in zirconium that the ethylene bridge, most likely due to a nonoptimal overlap between the indenyl π electrons and the metal d orbitals.

DFT energy profiles for the reactions between ethene or styrene and the IPs studied in this work fully justify the literature polymerization data on the basis of relative complex stabilities and competition between olefin retrodissociation and chain propagation. Employing the quantitative acidity scale developed in this work, it also becomes possible to rationalize the key differences between the energy profiles.

With the concepts quantitatively perfected in this work, one may be better prepared in tackling the task of fine-tuning the IP ligand sphere to generate more active catalysts both for ethene–styrene copolymers and for other co- and homopolymers. In particular, it would be interesting to explore the effect

of substituents on the aromatic rings that are capable of modifying the electronic structure of styrene by either inductive or conjugative effects. Similarly, the regioselectivity during styrene polymerization driven by similar catalysts may be explored further,[27,28] as well as the competition between propagation and β-hydrogen transfer during ethene polymerization by the corresponding *meso* species.[32]

■ EXPERIMENTAL SECTION

General Considerations. All the moisture-sensitive operations were carried out under a nitrogen atmosphere using standard Schlenk techniques. Dry solvents were freshly distilled before use. The toluene was kept under reflux in the presence of sodium for 48 h and then distilled under a nitrogen atmosphere. CH_2Cl_2 was purified by stirring for 1 h over calcium hydride and distilled under nitrogen. Et_2O was purified by stirring for 1 h over lithium aluminum hydride and distilled under nitrogen.

1,2-Bis(3-indenyl)ethane was purchased from Aldrich and used without further purification.

rac-(Ethylenebis(1-indenyl))zirconium dimethyl (*rac*-EBIZrMe$_2$), *rac*-(isopropylidenebis(1-indenyl))zirconium dimethyl (*rac*-iPr-BIZrMe$_2$), and *rac*-(ethylenebis(1-indenyl))hafnium dimethyl (*rac*-EBIHfMe$_2$) were prepared according to the procedures reported in the literature.[33,27]

Other materials and reagents available from commercial suppliers were generally used without further purification.

In Situ Preparation of Ion Pair Solutions. 0.01 M solutions in C_7D_8 (or C_6D_6) of 1/1 (mol/mol) *rac*-EBIZrMe$_2$, *rac*-EBIHfMe$_2$, or *rac*-iPrBIZrMe$_2$ and $B(C_6F_5)_3$ were prepared in a glovebox. In a typical procedure, 2 mg (2 mmol) of *rac*-EBIHfMe$_2$ and 3 mg (2 mmol) of $B(C_6F_5)_3$ were dissolved in 0.5 mL of C_7D_8 (or C_6D_6) in an NMR tube.

^{1}H NMR (400 MHz, δ, ppm, C_6D_6): −0.66 (s, HfCH$_3$, 3H), −0.35 (bs, CH$_3$B(C$_6$F$_5$)$_3$, 3H), 2.49−2.74 (m, CH$_2$ bridge, 4H), 4.97 (d, Cp H, 1H), 5.58 (d, Cp H, 1H), 5.72 (d, Cp H, 1H), 6.19 (d, Cp H, 1H), 6.20−7.32 (m, Ar, 8H).

^{1}H NMR (400 MHz, δ, ppm, C_6D_6): −0.60 (bs, CH$_3$B(C$_6$F$_5$)$_3$, 3H), −0.43 (s, ZrCH$_3$, 3H), 2.40−2.70 (m, CH$_2$ bridge, 4H), 5.11 (d, Cp H, 1H), 5.59 (d, Cp H, 1H), 5.91 (d, Cp H, 1H), 6.26 (d, Cp H, 1H), 6.32−7.33 (m, Ar, 8H).

^{1}H NMR (400 MHz, δ, ppm, C_6D_6): −0.59 (s, ZrCH$_3$, 3H), −0.21 (bs, CH$_3$B(C$_6$F$_5$)$_3$, 3H), 1.34−1.39 (d, C(CH$_3$)$_3$ bridge, 6H), 3.11 (d, Cp H, 1H), 4.76 (d, Cp H, 1H), 5.59 (d, Cp H, 1H), 6.05 (d, Cp H, 1H), 6.11−7.46 (m, Ar, 8H).

NMR Analysis. ^{1}H, ^{13}C, and ^{19}F spectra were recorded on a Bruker AM 400 spectrometer. Chemical shifts were referenced to residual solvent peaks (^{1}H, ^{13}C) or CFCl$_3$ (^{19}F). Variable-temperature spectra were recorded at temperature intervals of 10 °C over a range from −20 to +70 °C.

Two-dimensional ROESY NMR experiments were acquired using the standard four-pulse sequence, with a cycle delay of 1 s and mixing times of 250 and 800 ms.

PGSE NMR measurements were performed by using the standard stimulated echo pulse sequence[34] at 295 K without spinning. All of the spectra were acquired using 64 scans.

Computational Details. Gas-phase electronic structure calculations were carried out using the Gaussian09[35] suite of codes, employing BP86 density functional theory (DFT) with the local exchange−correlation potential by Vosko et al.[36] augmented in a self-consistent manner with Becke's exchange-gradient correction[37] and Perdew's correlation-gradient correction.[38] The basis set employed was LANL2DZ[39] with associate effective core potentials for second- and third-row atoms and SVP[40] for the first-row atoms. On the basis of the low value of the dielectric constant (2.38) for the solvent (toluene) commonly employed during polymerization, gas-phase calculations were deemed to be appropriate, as we would not expect a large separation between ions during the coordination and enchainment processes. Nevertheless, additional calculations employing the PCM model for toluene were carried out on the processes involving **3** and

ethene to put our strategy on more robust ground, the additional data being reported in Table TS1 in the Supporting Information. The latter quantitatively support our original choice, apart from a slight stabilization of the postenchainment product due to the solvent.

Geometries for most species (i.e., olefins, cations, IPs, olefin complexes, transition states (TS's) for chain propagation, and final products) were fully optimized, and the stationary points found were characterized by means of frequency calculations. For the latter species, putative structures for the energy minima and for chain propagation (CP) TS's were built using literature data[32] followed by either a complete geometrical relaxation or a partial relaxation keeping constrained the "active" part (e.g., the distances between metal and carbon atoms in the four-center TS for chain propagation, CP). The only difference with the latter procedure is related to the optimization of the TS for coordination of an olefin to the metal center of the ion pair, which was obtained by means of a constrained scan starting along the distance between one of the carbon atoms involved in the double bond and the metal, while optimizing the remaining degrees of freedom. The choice of paths to be explored via the relaxed scans was based on the results provided in ref 26, which suggested a route inserting the olefin between the counteranion and the alkyl substituent on the metal center (pathway C). Nevertheless, we also tested the path approaching the metal center from the external side of the anion for the Zr-containing species (pathway B), always finding a higher coordination barrier. In all cases, the initial geometry was chosen so to belong to a range of distances where the two moieties were weakly interacting. A complete optimization for a few of these TS's (mainly that involving ethene as the olefin together with the species bearing the ethylene bridge) was made complicated, however, by the intrinsic flexibility of the species, despite the attempt of using fully quadratic optimization algorithms. Thus, the TS geometry for these cases was obtained by employing a finer step size in a relaxed scan around the best TS candidate obtained previously. In all cases, the presence of a correct curvature for the potential energy surface around TS geometries was checked by performing frequency calculations. Importantly, we provide electronic energy differences rather than internal energy differences, as none of the studied processes involves the transfer of light atoms, the possible changes in vibrational frequencies being expected to cancel out to a large degree. A few tests carried out on selected species indeed supported this decision.

To gauge possible differences between the solution and gas-phase structures of organometallic precursors and IPs, which might have an effect on the estimated geometrical parameters, constrained optimizations were carried out by imposing experimentally derived distances between atoms. On the whole, only marginal changes were found between fully relaxed and constrained geometries for the above species, a strong indication of the robustness of both crystallographically and theoretically derived structures.

van der Waals volumes and radii for the IPs were estimated by assigning each atom a "catchment" sphere encapsulating it, whose radius was taken as the van der Waals radius,[41] sampling points with uniform distribution inside a cube sufficiently large to enclose the molecular volume built by the spheres, and multiplying the ratio between the number of points fallen inside the enveloping surface generated by the van der Waals spheres and the total sampled by the cube volume. In every case, we sampled a number of points sufficient to reduce the standard error of the volume estimate to roughly one part per thousand.

Whenever needed, NMR chemical shifts for carbon and hydrogen in the olefins were computed at the BP86/6-311+G(2d,2p)[42] level of theory in the gas-phase with the gauge independent atomic orbitals (GIAO)[43] using analytical derivatives.

■ ASSOCIATED CONTENT

Ⓢ Supporting Information

Figures and tables giving additional reaction profiles, a comparison between results obtained with and without a solvent model, NMR spectra, and Cartesian coordinates of the

stationary point structures optimized with DFT. This material is available free of charge via the Internet at http://pubs.acs.org.

■ AUTHOR INFORMATION

Corresponding Author

*E-mail: lizzo@unisa.it (L.I.); massimo.mella@uninsubria.it (M.M.).

Notes

The authors declare no competing financial interest.

■ REFERENCES

(1) Oliva, L.; Longo, P.; Izzo, L.; Di Serio, M. *Macromolecules* **1997**, *30*, 5616.

(2) Arai, T.; Ohtsu, T.; Suzuki, S. *Macromol. Rapid Commun.* **1998**, *19*, 327.

(3) Mella, M.; Izzo, L.; Capacchione, C. *ACS Catal.* **2011**, *1*, 1460.

(4) Deck, P. A.; Beswick, C. L.; Marks, T. J. *J. Am. Chem. Soc.* **1998**, *120*, 12167.

(5) Beswick, C. L.; Marks, T. J. *J. Am. Chem. Soc.* **2000**, *122*, 10358.

(6) Chen, E. Y.-X.; Marks, T. J. *Chem. Rev.* **2000**, *100*, 1391.

(7) Chen, Y.-X.; Metz, M. V.; Li, L.; Stern, C. L.; Marks, T. J. *J. Am. Chem. Soc.* **1998**, *120*, 6287.

(8) Yang, X.; Stern, C.; Marks, T. J. *Organometallics* **1991**, *10*, 840.

(9) Jia, L.; Yang, X.; Stern, C. L.; Marks, T. J. *Organometallics* **1997**, *16*, 842.

(10) Bochmann, M. *J. Organomet. Chem.* **2004**, *689*, 3982.

(11) Jordan, R. F. In *Advances in Organometallic Chemistry*; Stone, F. G. A., Robert, W., Eds.; Academic Press: New York, 1991; Vol. *32*, p 325.

(12) Brintzinger, H. H.; Fischer, D.; Mülhaupt, R.; Rieger, B.; Waymouth, R. M. *Angew. Chem., Int. Ed. Engl.* **1995**, *34*, 1143.

(13) Stahl, N. G.; Salata, M. R.; Marks, T. J. *J. Am. Chem. Soc.* **2005**, *127*, 10898.

(14) Zuccaccia, C.; Stahl, N. G.; Macchioni, A.; Chen, M.-C.; Roberts, J. A.; Marks, T. J. *J. Am. Chem. Soc.* **2004**, *126*, 1448.

(15) Siedle, A. R.; Newmark, R. A. *J. Organomet. Chem.* **1995**, *497*, 119.

(16) Yang, X.; Stern, C. L.; Marks, T. J. *J. Am. Chem. Soc.* **1994**, *116*, 10015.

(17) Song, F.; Lancaster, S. J.; Cannon, R. D.; Schormann, M.; Humphrey, S. M.; Zuccaccia, C.; Macchioni, A.; Bochmann, M. *Organometallics* **2005**, *24*, 1315.

(18) Piemontesi, F.; Camurati, I.; Resconi, L.; Balboni, D.; Sironi, A.; Moret, M.; Zeigler, R.; Piccolrovazzi, N. *Organometallics* **1995**, *14*, 1256.

(19) Horton, A. D.; de With, J.; van der Linden, A. J.; van de Weg, H. *Organometallics* **1996**, *15*, 2672.

(20) Winzor, D. J.; Jackson, C. M. *J. Mol. Recognit.* **2006**, *19*, 389.

(21) Lanza, G.; Fragalà, I. L.; Marks, T. J. *J. Am. Chem. Soc.* **2000**, *122*, 12764.

(22) Xu, Z.; Vanka, K.; Firman, T.; Michalak, A.; Zurek, E.; Zhu, C.; Ziegler, T. *Organometallics* **2002**, *21*, 2444.

(23) McNaught, A. W. A. D. *IUPAC Compendium of Chemical Terminology*; Blackwell Scientific: Oxford, U.K., 1997.

(24) Chan, M. S. W.; Vanka, K.; Pye, C. C.; Ziegler, T. *Organometallics* **1999**, *18*, 4624.

(25) Xu, Z.; Vanka, K.; Ziegler, T. *Organometallics* **2003**, *23*, 104.

(26) Lanza, G.; Fragalà, I. L.; Marks, T. J. *Organometallics* **2002**, *21*, 5594.

(27) Galdi, N.; Izzo, L.; Oliva, L. *Organometallics* **2010**, *29*, 4434.

(28) Correa, A.; Galdi, N.; Izzo, L.; Cavallo, L.; Oliva, L. *Organometallics* **2008**, *27*, 1028.

(29) Chan, M. S. W.; Ziegler, T. *Organometallics* **2000**, *19*, 5182.

(30) Correa, A.; Talarico, G.; Cavallo, L. *J. Organomet. Chem.* **2007**, *692*, 4519.

(31) Yang, S. H.; Jo, W. H.; Noh, S. K. *J. Chem. Phys.* **2003**, *119*, 1824.

(32) Caporaso, L.; Galdi, N.; Oliva, L.; Izzo, L. *Organometallics* **2008**, *27*, 1367.

(33) Balboni, D.; Camurati, I.; Prini, G.; Resconi, L.; Galli, S.; Mercandelli, P.; Sironi, A. *Inorg. Chem.* **2001**, *40*, 6588.

(34) Valentini, M.; Rüegger, H.; Pregosin, P. S. *Helv. Chim. Acta* **2001**, *84*, 2833.

(35) Trucks, M. J.; Frisch, G. W.; Schlegel, H. B.; Scuseria, G. E.; Robb, M. A.; Cheeseman, J. R.; Montgomery, J. A., Jr.; Vreven, T.; Kudin, K. N.; Burant, J. C.; Millam, J. M.; Iyengar, S. S.; Tomasi, J.; Barone, V.; Mennucci, B.; Cossi, M.; Scalmani, G.; Rega, N.; Petersson, G. A.; Nakatsuji, H.; Hada, M.; Ehara, M.; Toyota, K.; Fukuda, R.; Hasegawa, J.; Ishida, M.; Nakajima, T.; Honda, Y.; Kitao, O.; Nakai, H.; Klene, M.; Li, X.; Knox, J. E.; Hratchian, H. P.; Cross, J. B.; Adamo, C.; Jaramillo, J.; Gomperts, R.; Stratmann, R. E.; Yazyev, O.; Austin, A. J.; Cammi, R.; Pomelli, C.; Ochterski, J. W.; Ayala, P. Y.; Morokuma, K.; Voth, G. A.; Salvador, P.; Dannenberg, J. J.; Zakrzewski, V. G.; Dapprich, S.; Daniels, A. D.; Strain, M. C.; Farkas, O.; Malick, D. K.; Rabuck, A. D.; Raghavachari, K.; Foresman, J. B.; Ortiz, J. V.; Cui, Q.; Baboul, A. G.; Clifford, S.; Cioslowski, J.; Stefanov, B. B.; Liu, G.; Liashenko, A.; Piskorz, P.; Komaromi, I.; Martin, R. L.; Fox, D. J.; Keith, T.; Al-Laham, M. A.; Peng, C. Y.; Nanayakkara, A.; Challacombe, M.; Gill, P. M. W.; Johnson, B.; Chen, W.; Wong, M. W.; Gonzalez, C.; Pople, J. A. *Gaussian 09*; Gaussian, Inc., Pittsburgh, PA, 2009.

(36) Vosko, S. H.; Wilk, L.; Nusair, M. *Can. J. Phys.* **1980**, *58*, 1200.

(37) Becke, A. D. *Phys. Rev. A* **1988**, *38*, 3098.

(38) Perdew, J. P. *Phys. Rev. B* **1986**, *33*, 8822.

(39) Hay, P. J.; Wadt, W. R. *J. Chem. Phys.* **1985**, *82*, 299.

(40) Schafer, A.; Huber, C.; Ahlrichs, R. *J. Chem. Phys.* **1994**, *100*, 5829.

(41) Bondi, A. *J. Phys. Chem.* **1964**, *68*, 441.

(42) Raghavachari, K.; Trucks, G. W. *J. Chem. Phys.* **1989**, *91*, 2457.

(43) McWeeny, R. *Phys. Rev.* **1962**, *126*, 1028.